Cement and Concrete Research 126 (2019) 105917

Contents lists available at ScienceDirect

Cement and Concrete Research

journal homepage: www.elsevier.com/locate/cemconres

Prediction of autogenous shrinkage of cement pastes as poro-visco-elastic deformation

Zhangli Hu[b,*], Mateusz Wyrzykowski[b], Karen Scrivener[a], Pietro Lura[b,c]

[a] Laboratory of Construction Materials, EPFL, Lausanne CH-1015, Switzerland
[b] Concrete/Construction Chemistry Laboratory, Empa, Dübendorf CH-8600, Switzerland
[c] Institute for Building Materials, ETH Zurich, Zurich CH-8092, Switzerland

ARTICLE INFO

Keywords:
Autogenous shrinkage
Poro-visco-elastic response
Poromechanics models
Generalized Kelvin-Voigt model
Parameters verification

ABSTRACT

Precise and robust predictions of autogenous shrinkage of high performance concrete are essential to limit self-induced stresses and cracking in modern concrete structures. This paper presents predictions of autogenous shrinkage for three cement pastes of different compositions by considering first only the poro-elastic deformation and then including also the poro-visco-elastic response. This study used experimentally-determined parameters for the material properties of both the elastic and the visco-elastic components, which ensured the reliability of the calculations. The prediction of the poro-visco-elastic response of the material to the internal stress was performed using a generalized Kelvin-Voigt model that also considered aging. It is found that, while the poro-elastic calculations systematically underestimates the measured shrinkage, predictions with the inclusion of the viscous response overestimates the shrinkage.

1. Introduction

Autogenous shrinkage of cement-based materials is the unrestrained volume contraction occurring in isothermal conditions without any moisture exchange or external load [1]. It can reach high magnitude especially in high performance concrete with low water-to-cement ratio (w/c) [2], where it may lead to cracking. Investigations on autogenous shrinkage of cementitious materials have been carried out for several years and considerable effort has been dedicated to formulate reliable models for predicting autogenous shrinkage (e.g., [3–5]).

Existing prediction methods for autogenous shrinkage can be divided into two main categories: (1) empirical and semi-empirical models and (2) mechanistic models.

Empirical or semi-empirical models are models obtained via regression analysis of experimental data [6–8]. The parameters usually taken into account are the mixture properties (e.g., w/c, mineral compositions of cement and aggregates, stiffness of aggregates, paste or aggregate volume fraction) and the compressive strength of the concrete [6,8,9].

In mechanistic models, poromechanics approaches for unsaturated porous materials based on changes of pore fluid pressure as the main driving force are commonly used to predict autogenous shrinkage (e.g., [10–12]). Most of the models for predicting the pore fluid pressure are based on the Kelvin-Laplace equation [13]. This equation is valid both when changes in capillary pressure or in disjoining pressure are considered as the physical mechanism causing shrinkage [14,15]. After obtaining the pore fluid pressure, the resulting strain is calculated either by analytical models (e.g., multi-scale modelling with self-consistent scheme homogenization and Mori-Tanaka homogenization [3]) or by numerical models (e.g., finite element method (FEM) homogenization [10]).

However, predictions of autogenous shrinkage by using either analytical or numerical methods in most cases underestimated shrinkage [10,11]. Therefore, attention has been paid to identify the reason for these discrepancies.

Since cement paste displays visco-elastic behavior under stress, such behavior is also likely to occur under the action of internal stress due to pore fluid pressure, as suggested already in [11,16–18]. In a recent metastudy [18], it was observed that autogenous deformation of cementitious materials with w/c below about 0.5 does not cease together with hydration, but continues over the long term as a logarithmic function of time. Hence, it was concluded that long-term autogenous shrinkage is due to the creep response to the action of equivalent (in terms of the Biot-Bishop formulation) pore pressure.

Following this hypothesis and the superposition principle of strains (e.g. [19]), autogenous shrinkage (neglecting thermal dilation because of the isothermal conditions and neglecting possible damage, e.g. micro-cracks) can be expressed as:

* Corresponding author at: Concrete/Construction Chemistry Laboratory, Empa, Dübendorf CH-8600, Switzerland.
E-mail address: zhangli.hu@empa.ch (Z. Hu).

https://doi.org/10.1016/j.cemconres.2019.105917
Received 25 April 2019; Received in revised form 30 September 2019; Accepted 4 October 2019
0008-8846/ © 2019 Elsevier Ltd. All rights reserved.

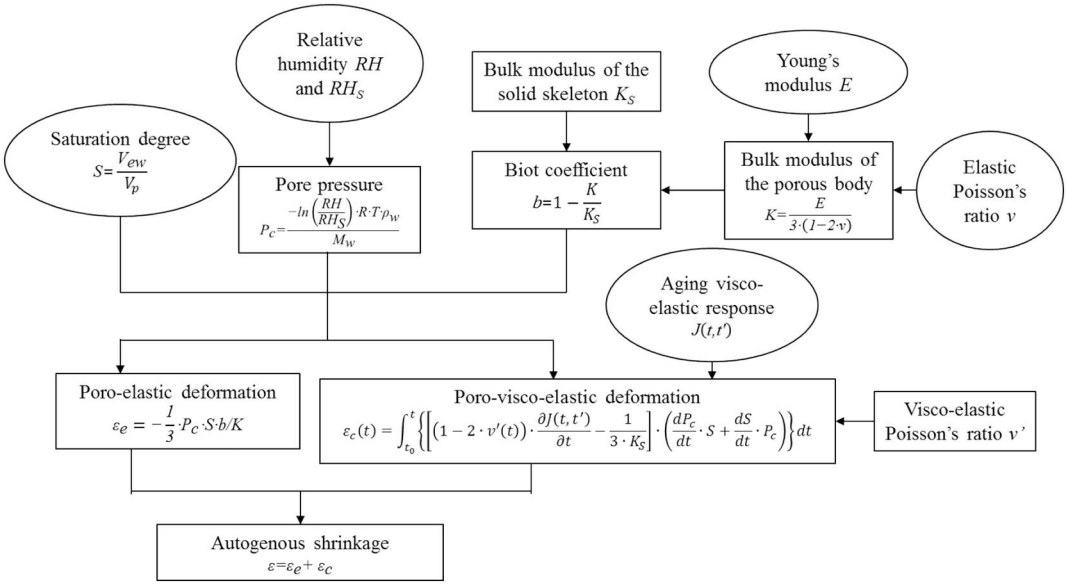

Fig. 1. Diagram of the prediction process of autogenous shrinkage. Oval shapes represent input obtained from experiments and rectangles represent modelling steps.

$$\varepsilon = \varepsilon_e + \varepsilon_c \tag{1}$$

where: ε [μm/m] is the total autogenous shrinkage occurring after setting (in the solid material), ε_e [μm/m] is the (poro-) elastic deformation and ε_c [μm/m] is the contribution of creep (visco-elastic) deformation.

The assumption that a part of the measured shrinkage in cementitious system is due to creep under sustained internal load (Eq. (1)) has been proposed for the case of autogenous shrinkage by Hua et al. [12,20] and later extended by Grasley and Leung [21] for the general case of desiccation shrinkage (autogenous and/or drying shrinkage). This approach was validated in [21] with experiments on drying cement pastes at early age. While our work follows the same fundamental principle (and hence it could be extended to the case of drying as in [21]), it is devoted specifically to the case of autogenous shrinkage. The parameters used in modelling (mechanical properties, moisture state evolution, basic creep, etc.) are obtained on the same cement pastes in an extensive experimental study. The validation of the approach is carried out based on experimental measurements of autogenous shrinkage of blended cement pastes, see Fig. 1. Additionally, a sensitivity analysis of the effect of different parameters governing autogenous shrinkage and corresponding creep is carried out.

2. Prediction method

The whole prediction process of linear autogenous shrinkage is illustrated in Fig. 1. In the diagram, the parameters and the involved equations are also shown in each parameter block. The model parameters determined by experiments in this study are: saturation degree S [−], relative humidity RH [−] and relative humidity decrease due to ions present in the pore solution RH_S [−], Young's modulus E [GPa], elastic Poisson's ratio ν [−] and aging visco-elastic response $J(t,t')$. Note that the equations listed in the diagram may vary according to the different poromechanics models applied. A more detailed explanation is given in the following sections.

2.1. Poro-elastic prediction

The basis of most poromechanics models applied to the prediction of shrinkage in cementitious materials (e. g., [11,12,16]) is the Biot-Bishop approach [22], originally developed for soils.

In the Biot-Bishop approach [22], four parameters need to be determined to predict the linear strain ε_e [m/m]: saturation degree S, capillary pressure P_c [GPa], bulk modulus K [GPa] of the porous material and bulk modulus of the solid body K_S [GPa], see Eq. (2).

$$\varepsilon_e = -\frac{1}{3}\bullet P_c\bullet S\bullet b/K = -\frac{1}{3}\bullet P_c\bullet S\bullet\left(\frac{1}{K}-\frac{1}{K_S}\right) \tag{2}$$

b is the Biot coefficient, defined as $1-K/K_S$. The capillary pressure can be estimated from the RH evolution of the system using the Kelvin-Laplace equation. It should be stressed that this approach in the form expressed with Eq. (2) is only relevant for the ultimate poro-elastic deformation of an inert material. In the case of autogenous shrinkage, it needs to be used in a differential form to account for the evolution of material properties due to hydration (see e.g. [17]). Furthermore, the differential form is also required if one considers the visco-elastic response in addition to the elastic part [19].

The central term in the poro-elastic approach is the negative pore fluid pressure acting on the solid skeleton and leading to contraction upon desaturation. In the form used in classical Biot-Bishop approach, Eq. (2), it takes the form of approximated (after neglecting the contribution of the air pressure changes) averaged pore pressure acting on the solid skeleton, $P_C{\cdot}S$. According to [18], the effective equivalent pore pressure, after accounting for the Biot's coefficient b, reaches about 15–20 MPa for a concrete with w/c of 0.2. This pressure is then treated in [18] as a stress leading to long-term creep response.

Another development was proposed by Coussy et al. [23]. In their approach, an equivalent pore pressure takes the place of the average pore pressure, taking also into account the contribution of the interface energy due to adsorbed fluid. The resulting equation is as follows [23]:

$$\varepsilon_e = -\frac{1}{3}\bullet(SP_c+U)\bullet\left(\frac{1}{K}-\frac{1}{K_S}\right) = -\frac{1}{3}\bullet\left(SP_c+\int_S^1 P_c(S)dS\right)\bullet\left(\frac{1}{K}-\frac{1}{K_S}\right) \tag{3}$$

where U [GPa] is the interface energy. For drying shrinkage, this modification may change substantially the final results at low RH, but is expected to have only limited effect at the RH levels encountered in autogenous conditions [24].

Both the classical Biot-Bishop approach [22] and Coussy's method [23] were used in the poro-elastic predictions in this paper, since they consider different driving forces. All the parameters needed for the predictions according to the two approaches are as indicated in Fig. 1.

The approaches for determining different parameters in the calculation are explained in the following.

2.1.1. Capillary pressure

The capillary pressure P_C used in the model evolves according to the Kelvin-Laplace equation based on the measured RH, see Eq. (4).

$$P_c = \frac{-\ln\left(\frac{RH}{RH_S}\right)\bullet R\bullet T\bullet \rho_w}{M_w} \tag{4}$$

This equation assumes perfect wetting between pore fluid and solids (contact angle of 0°). $R = 8.314\,J/(mol{\cdot}K)$ is the ideal gas constant. In this paper, the temperature is $T = 293.15\,K$, the molar mass of water $M_w = 0.01802\,kg/mol$ and density of water $\rho_w = 1000\,kg/m^3$ are used for the pore fluid [13]. RH and RH_S were determined by water activity sensors for both the cement pastes and the extracted pore solution, see [25].

2.1.2. Saturation degree

The saturation degree is the volume fraction of the evaporable water (V_{ew}) divided by the total porosity (V_p), see Eq. (5) [11].

$$S = \frac{V_{ew}}{V_p} \tag{5}$$

To find the saturation degree S, the porosity and the water content or the emptied pores volume need to be known. Conventionally, there are two classes of experimental methods for determining S: destructive and non-destructive. The destructive approach requires to remove water and to determine a dry reference state, e.g., water vapor sorption isotherms measurements [3]. With water vapor sorption isotherms, it is not possible to determine the S of an early-age sample that undergoes hydration, as drying to a reference state is a time-lapsed process occurring in parallel to hydration. A possible solution for this is using an equivalent system [26] that does not undergo any hydration during the test to emulate the early-age system. A non-destructive approach like ^{1}H nuclear magnetic resonance (NMR) [27], on the other hand, does not require drying to a reference state, as the method probes all water in a sample almost instantaneously at any time point.

The estimation of S can also be done with Powers' model combined with either experimental data on mineralogy or with the phase assemblage calculated from e.g. Gibbs Energy Minimization (GEMs) [11].

In any case, the definition of saturation degree depends on the arbitrarily-assumed reference state [28]. In the method involving drying to a reference (dry) state, this will correspond to the drying regime chosen. In the ^{1}H NMR method, or in theoretical estimations with Powers' model, the issue still persists and regards the choice of which water populations should be included in the calculation of the saturation degree. In other words, the problem converges to choosing which water populations should be considered to average the pore fluid pressure acting on the solid skeleton.

In this paper, to quantify the amount of evaporable water that contributes to the saturation degree, both Powers' model and ^{1}H NMR are employed. According to Powers' model, the evaporable water [29] is the water lost after drying at 105 °C. Powers divided the evaporable water into gel water and capillary water and distinguished it from non-evaporable water that is a part of the hydrated solids. According to recent ^{1}H NMR findings, the water within cement paste can be classified into different water classes: interlayer water, gel water and capillary water [30,31]. It should be however stressed, that the gel and capillary water determined with NMR are not equivalent to the evaporable water defined by Powers. The difference mainly regards the fact that part of the C-S-H interlayer water can be lost at 105 °C and is to a certain extent mobile, i.e. it can exchange with gel water as a function of temperature or applied stresses [32].

In this study, in order to assess the effect of the different definitions of saturation degree and hence its influence on averaging the pore pressure, three different definitions were used, S_{Powers}, $S_{NMRinter}$, S_{NMR}, corresponding to the Powers' model, NMR measurements including interlayer water, and NMR measurements neglecting interlayer water, respectively:

$$S_{Powers} = \frac{V_{ew}(\alpha)}{V_p(\alpha)} = \frac{V_{cw}(\alpha) + V'_{gw}(\alpha)}{V_{cw}(\alpha) + V'_{gw}(\alpha) + V_{cs}(\alpha)} \tag{6a}$$

$$S_{NMRinter} = \frac{V_{ew}(\alpha)}{V_p(\alpha)} = \frac{V_{cw}(\alpha) + V_{gw}(\alpha) + V_{inter}(\alpha)}{V_{cw}(\alpha) + V_{gw}(\alpha) + V_{inter}(\alpha) + V_{cs}(\alpha)} \tag{6b}$$

$$S_{NMR} = \frac{V_{ew}(\alpha)}{V_p(\alpha)} = \frac{V_{cw}(\alpha) + V_{gw}(\alpha)}{V_{cw}(\alpha) + V_{gw}(\alpha) + V_{cs}(\alpha)} \tag{6c}$$

where: V_{cw} [ml/ml], V_{gw} [ml/ml] and V_{inter} [ml/ml] are the volume fraction of the capillary water, gel water and interlayer water, respectively. V'_{gw} [ml/ml] is the volume fraction of the gel water classified according to Powers' method. V_{cs} [ml/ml] is the chemical shrinkage or the emptied pore volume fraction. All of them depend on the degree of hydration of the system α and the dependence is unique only in sealed conditions, in which the pores are emptied by chemical shrinkage only. The porosity in Eqs. (6a), (6b), and (6c) are considered as the sum of the volume of all evaporable water and of the chemical shrinkage. In Eq. (6a), the calculation of the porosity was based on Powers' model. The detailed calculation of evaporable water and chemical shrinkage based on Powers' model for SCM-blended systems can be seen in Appendix A. In Eq. (6b) and (6c), to obtain the volume fraction of capillary water, gel water and interlayer water from ^{1}H NMR, signal fractions of different types of water obtained from ^{1}H NMR [25] were transformed to volume fractions of different water populations in the systems with the assumption that all types of water share the same density of $1\,g/cm^3$. This assumption may lead to a slight overestimation of water volume, considering that the density of bound water may be actually higher (the density of physically bound was found to be about $1.15\,g/cm^3$ in [33,34]). This higher density of part of the water corresponds to the upper limit of the overestimation of the volume (i.e. by 15–25%) due to the fact that only the most confined (interlayer) water is expected to have such higher density (in [33] such higher density is found for water desorbing below 33%RH).

The most common methods used for obtaining the porosity are water absorption [35], mercury intrusion porosimetry (MIP) and nitrogen adsorption and desorption isotherms [36]. On the one hand, MIP and nitrogen adsorption require drying the samples prior to the measurements, which may damage the pore structure, especially at early ages. On the other hand, as already mentioned, traditional gravimetric methods (by weighing a sample at a certain state and then after drying) are not applicable for systems that undergo rapid hydration, due to the time necessary for saturating or drying of the samples while they still hydrate. Secondly, neither MIP nor nitrogen adsorption/desorption isotherms are able to quantify the total amount of pores, since mercury and nitrogen cannot measure the whole range of pore sizes (i.e., the minimum entry pore diameter of MIP at 400 MPa is around 3.6 nm assuming a contact angle of 120°, while nitrogen adsorption is not applicable to pores above 200 nm) [37]. To avoid these limitations, in this paper, the total porosity obtained from combining ^{1}H NMR (water-filled pores) and chemical shrinkage (empty pores) was compared to the estimation from Powers' model.

2.1.3. Bulk moduli

The bulk moduli of the porous material and of the solid skeleton, K and K_S, describe the compressibility of the porous material and of the solids, respectively. The hydration-dependent K can be determined from the Young's modulus E and the Poisson's ratio ν, see Eq.(7), in which the Poisson's ratio decreases from 0.5 before setting (value for an incompressible fluid [38]) and stabilizes at values around 0.18–0.25 after about 1 day of hydration [11,39].

$$K = \frac{E}{3\bullet(1 - 2\,\nu)}. \tag{7}$$

For cement paste, K_S is reported to be in the range between 38 and

55 GPa, depending on the bulk modulus of all the solid phases in the system, among which the largest uncertainty is the bulk modulus of the intrinsically-porous C-S-H [40]. In principle, K_S should be approximately constant or should slightly decrease at early ages due to the lower Young's modulus of hydrated phases compared to the anhydrous phases [48]. In the predictions, for simplicity, constant K_S was used (as in [11]).

According to Eq. (7), Young's modulus and Poisson's ratio are the two parameters needed for calculating the bulk modulus of the porous body. The Young's modulus was based on the results of static Young's modulus measurements. The Poisson's ratio was taken from [39], where it was obtained from dynamic measurements of elastic and shear modulus with ultrasound resonance spectroscopy according to ASTM C215 [41] on a w/c 0.30 cement paste (see Fig. 4).

The parameters used in these models were all determined from experiments, except for K_S. In addition, the Biot-Bishop approach was used as a reference method for studying the effect of the following parameters:

1) Poisson's ratio determined experimentally in [39] or with an assumed constant value of 0.22;
2) saturation degree either determined based on ^{1}H NMR and chemical shrinkage or using Powers' model;
3) constant K_S of 44 GPa or upper and lower values 38 GPa and 55 GPa [40].

2.2. Poro-visco-elastic prediction

In the empirical method proposed by Hua et al. [12], the linear autogenous shrinkage included both an elastic and a visco-elastic component, which were then combined based on Boltzmann's superposition principle (see Eq. (1)). The parameters governing the visco-elastic part were determined by comparison with the experimental data (minimizing the error). This simulation ignored aging of the creep compliance, and resulted in an overestimation of the overall autogenous shrinkage. A further development was proposed by Gawin et al. [16] who applied the microprestress-solidification theory by Bazant et al. [42] together with the effective stress principle. However, also in the latter model, creep properties were obtained by means of fitting the total deformation. A prominent development in modelling of (aging) creep accompanying drying was presented by Grasley and Leung [21] who calibrated the poro-visco-elastic model based on the independent companion uniaxial compressive creep tests. A similar approach was also followed here.

To consider the visco-elastic component in the autogenous shrinkage prediction, the most challenging task, especially at early ages, is to find a way to deal with aging with changing stresses (changes of pore pressure assumed as the driving force of autogenous shrinkage). At the macroscopic scale, pore fluid pressure is a hydrostatic load; the stress state induced by self-desiccation (or in general, by drying) is different than in uniaxial compression or tension tests commonly used to investigate creep of concrete. Due to its relative simplicity and relevance for practice, the uniaxial compressive creep test has been used most widely in studies of visco-elastic deformation of cementitious materials [43]. The experimental campaign and a discussion of the creep of the cementitious materials studied were presented in an accompanying paper [44].

In this paper, the visco-elastic equivalent bulk modulus was calculated from the creep compliance measured in uniaxial compression on sealed samples and the ratio of the transversal to axial creep strains (also referred to as the visco-elastic Poisson's ratio) was assumed equal to the elastic Poisson's ratio (see discussion later). The creep compliance was obtained by subtracting from the total deformation of loaded sealed samples the quasi-instantaneous part occurring directly after loading and further subtracting the linear autogenous shrinkage part measured on the corrugated tubes ([45]) in parallel. The calculation of the visco-elastic deformation function was carried out with the generalized Kelvin-Voigt model and the input stress of the average pore pressure $S{\cdot}P_c$. The generalized Kelvin-Voigt model employed in this paper consists of a series of three Kelvin-Voigt units and an additional dashpot. The Kelvin-Voigt units can be used to model the short-term creep; the additional dashpot in series represents long-term creep, which is proportional to time (or degree of hydration) in the model. The description of the coefficients in the model is identified as follows: $E_n(t)$ [MPa] are the aging moduli of the springs in the individual Kelvin-Voigt unit, n is 1, 2 and 3; t [days] is the time; $\eta_n(t)$ are the viscosities of the dashpots in the corresponding Kelvin-Voigt unit. The additional dashpot has viscosity η_0. τ_n [day] is the retardation time.

The evolution of the parameters (stiffness of springs and viscosity of dashpot) in the generalized Kelvin-Voigt chains model were obtained by calibrating with the experimental results presented in [44]. The parameters used in the Kelvin-Voigt chain to predict the visco-elastic component for the three systems studied in this paper are listed in Section 4. The model was validated by predicting the creep strain of specimens under stepwise loading with the same parameters obtained from the creep results of specimens under constant loading and the results were then compared with the experiments under stepwise loading.

The creep component of the linear autogenous shrinkage was predicted with the following equation:

$$\varepsilon_c(t) = \int_{t_0}^{t} \left\{ \left[(1 - 2{\bullet}\nu'(t)){\bullet}\frac{\partial J(t,t')}{\partial t} - \frac{1}{3{\bullet}K_S} \right]{\bullet}\left(\frac{dP_c}{dt}{\bullet}S + \frac{dS}{dt}{\bullet}P_c \right) \right\} dt \tag{8}$$

where: t, t_0 and t' are the current time, reference time and the loading time, respectively; ν' is the visco-elastic Poisson's ratio (the ratio between transverse and longitudinal visco-elastic strain), $J(t,t')$ is the specific basic creep compliance (uniaxial).

3. Materials and experimental methods

To validate the prediction method, three cement pastes were studied, in which Portland cement, quartz filler and class F fly-ash were the same as used in [44]. Pastes of ordinary Portland cement (PC), fly-ash-blended cement with 40% by mass of solid (FA40) and quartz-blended cement with substitution level of 46.7% by mass of solid (QZ40) with the same water-to-solid ratio of 0.35 were prepared. The volume fraction of fly-ash and quartz replacing cement are the same in FA40 and QZ40 (49%). The pastes were mixed for 2 min with a vacuum mixer at mixing speed of 450 rpm.

The experimental methods, including autogenous shrinkage, internal RH, Young's modulus and creep were described in detail in the accompanying papers [44,46]. The autogenous shrinkage was determined using the corrugated tubes method [47] with automatic measurements on a dilatometer equipped with LVDTs and immersed in a silicone-oil bath for better temperature stability and for avoiding the loss of moisture from the samples. The details of the method are presented in [45]. The strains were calculated assuming time zero at the time of final set determined by Vicat needle. The internal RH and the RH_S were measured using water activity sensors on freshly cast cement paste samples and extracted pore solution, respectively [25]. The Young's modulus was measured using static measurements in compression according to the Swiss standard [48] and the uniaxial creep in compression was measured using a creep frame equipped with a lever mechanism [44,46]. All experiments were performed in temperature-controlled rooms at 20 ± 0.3 °C. The samples used in all experiments were properly sealed, ensuring negligible evaporation of water and temperature change during the testing period. The overall moisture loss of the specimens after 1 month was less than 0.3% of the initial mass of the specimen. The relative amount of different water populations in PC and QZ40 was measured using ^{1}H NMR as described in [25]. A Bruker

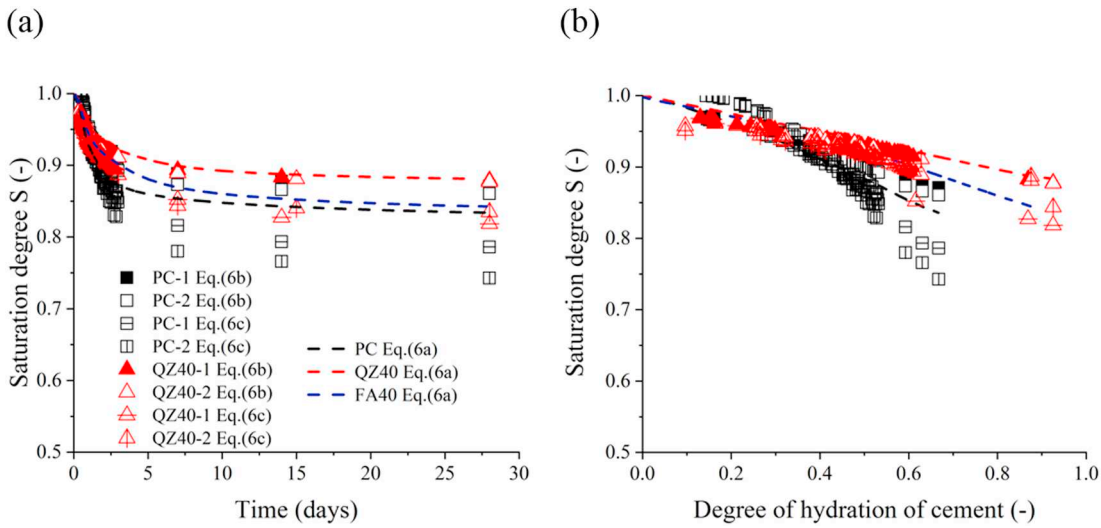

Fig. 2. Saturation degrees of different systems calculated either with Powers' model (Eq. (6a)) or based on ^{1}H NMR and chemical shrinkage (Eq. (6b) – including interlayer water, Eq. (6c) – excluding interlayer water): (a) as a function of time; (b) as a function of degree of hydration. The calculations using NMR results are presented for duplicate samples (indexes 1 and 2).

Minispec benchtop NMR spectrometer with operating frequency of 7.5 MHz was used. The quantification of capillary water, gel water, interlayer water and solid water were performed by introducing Carr-Purcell-Meiboom-Gill (CPMG) and quadrature echo sequences. However, the NMR measurements could not be performed on the paste containing fly ash, due to the paramagnetic impurities (typically Fe^{3+}) present in the fly ash powders.

4. Parameters from experiments

4.1. Saturation degree

The saturation degree of the three systems determined with the three approaches presented in Eqs. (6a), (6b), and (6c) are shown in Fig. 2. The water fraction in FA40 could not be measured with ^{1}H NMR due to too fast relaxation because of the high iron content in the system [31]. Therefore, for the method using ^{1}H NMR and chemical shrinkage, only results of PC and QZ40 are presented. The details of the calculation of the saturation degree, in particular of the blends of cement with quartz or fly ash are presented in Appendix A.

As expected, PC had in all cases the lowest saturation degree compared to QZ40 and FA40. When Powers' model and the estimation based on combining ^{1}H NMR and chemical shrinkage are compared, larger differences were found when interlayer water was excluded (Eq. (6c)) and only gel and capillary water populations were considered as resolved by NMR. This proves that gel and capillary water estimations based on the dry reference state at 105 °C do not correspond well to the capillary and gel water populations observed with NMR and that part of the interlayer water belongs to the evaporable water at 105 °C. Another possible reason of the differences between the different methods is that Powers' model (published in 1946) [49] is based on Portland cements produced at that time. Differences in the cement mineralogy and especially in the fineness may explain at least partially the different results [50,51].

Another recent finding from ^{1}H NMR shows that the evolution of the total volume fraction of water is not linear with the degree of hydration at early ages, contrary to what is assumed in Powers' model [37]. In fact, higher desaturation, understood as a loss of free water, than dictated by a linear trend is found in [37] at low hydration degrees (below about 0.3–0.4). This is consistent with our results.

In any case, the maximum difference of the saturation degree between Powers' model and the NMR method was around 0.07, not considerably more than the scatter from the latter method (see the difference between duplicate samples of PC calculated with Eq. (6c) – black empty squares in Fig. 2a).

4.2. Average pore fluid pressure

The average pore fluid pressure (approximated as $S{\cdot}P_c$) is assumed as the driving force both for the elastic response and the visco-elastic response of the materials, as shown in Fig. 3. S is taken from Powers' model due to the unavailability of ^{1}H NMR results of the FA40 system. For ease of representation, the average pore pressure (negative) calculated from the average internal RH and RH_S was plotted as a positive value in Fig. 3. As cement hydration goes on, the magnitude of the pressure increases, following the Kelvin equation. The maximum magnitude of the pore pressure reaches around 14 MPa, which is considerably lower than the triaxial compressive strength [52]; therefore, it can be assumed that the material remains in the linear elastic regime.

4.3. Other parameters

4.3.1. Poisson's ratio

The dynamic Young's modulus, the shear modulus and the corresponding (elastic) Poisson's ratio of cement paste up to 10 days are plotted in Fig. 4. Note that the Poisson's ratio was taken from [39], where it was determined experimentally with resonance ultrasound spectroscopy (i.e. dynamic measurements) on an ordinary Portland cement paste with w/c of 0.30. The Poisson's ratio decreased sharply during the first day, from about 0.32 to 0.24. After 2 days, the evolution of the Poisson's ratio was much slower, decreasing asymptotically to about 0.22. The development of the Poisson's ratio at early ages is found to be dominated by the fluid phase response before the solid phases start to percolate, and then by the solid phase response [53]. The experimental data were fitted with an exponential equation, which was later used in the autogenous shrinkage prediction.

4.3.2. Visco-elastic Poisson's ratio

The visco-elastic Poisson's ratio is defined here as the ratio of the transversal to the longitudinal visco-elastic deformation. The experimental determination of this variable is very challenging due to relatively small deformations in the transversal direction during uniaxial creep tests. A further issue regards the question whether only creep deformations or total deformations (creep + elastic) should be

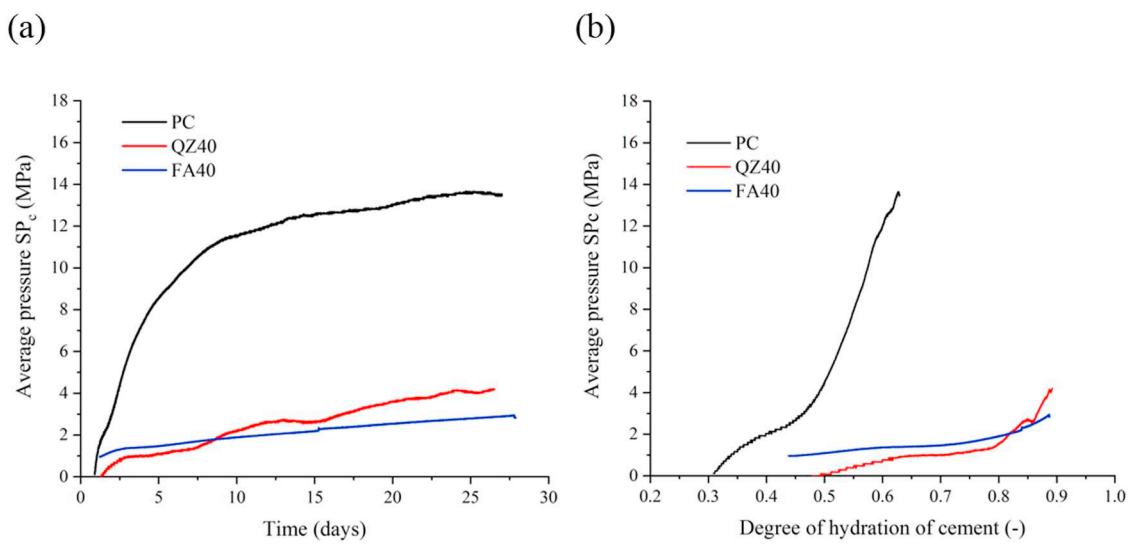

Fig. 3. Average pore pressure in two systems: (a) as a function of time; (b) as a function of degree of hydration (with *S* from Powers' model).

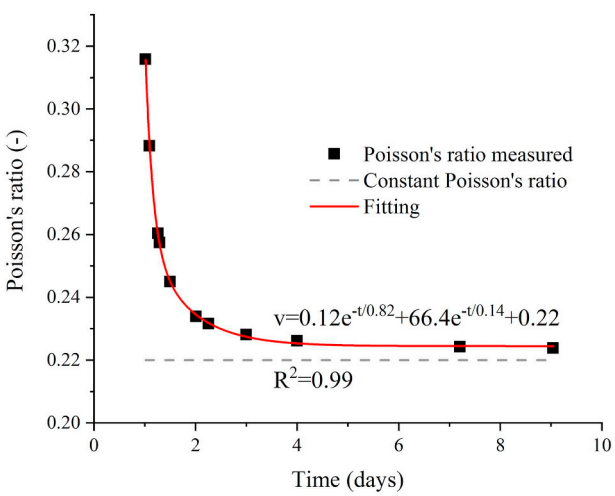

Fig. 4. Poisson's ratio measured with ultrasound resonance spectroscopy in [39] and fitted with a trend line compared to the constant Poisson's ratio of 0.22.

considered in evaluating the ratio (see [54,55]). In the literature, a large scatter is reported for the visco-elastic Poisson's ratio, with contradictory trends (both increase and decrease over time), but for mature concrete values around 0.15 to 0.2 are reported [55]. As reported in [56], the visco-elastic Poisson's ratio is similar to the elastic Poisson's ratio at stress levels lower than 40% of the compressive strength.

In [57], the visco-elastic Poisson's ratio was determined based on FEM simulations on evolving microstructures considering the dissolution/precipitation of cement particles during hydration and the intrinsic visco-elasticity of the C-S-H. The values of visco-elastic Poisson's ratio found were between about 0.2–0.35 and an increasing trend was found during hydration. It should be however noted that the values/trends found in [57] strongly depended on the intrinsic visco-elastic properties of the C-S-H assumed in the simulations (two different assumed functions for either visco-elastic Young or shear modulus led to considerably different results) and in addition strongly depended on the simulated loading ages (two ages were modelled in [57]: 1 and 7 d).

On the other hand, Aili et al. [55] argued based on micromechanical modelling, where viscoelastic deformations were downscaled to the C-S-H level, that the elastic Poisson's ratio can be used with reasonable accuracy also for describing the visco-elastic Poisson's ratio.

Therefore, in view of the last argument and in lack of any reliable data on the visco-elastic Poisson's ratio, we assumed in the simulations that it is equal to the elastic one. Two cases were considered consequently, corresponding to the two different evolutions of (elastic) Poisson's ratio as shown in Fig. 4: with constant (0.22) or decreasing Poisson's ratio.

5. Prediction results and discussions

5.1. Poro-elastic prediction

5.1.1. Comparison of the prediction from three different methods

The predicted elastic response of the autogenous shrinkage by the three different models (Coussy's method and Biot-Bishop method with either constant or evolving Poisson's ratio) and the measured autogenous shrinkage for the three cement pastes are shown in Fig. 5. In these simulations, saturation degree determined with Eq. (6a) was used.

The autogenous shrinkage of PC was almost 5 times higher than that of QZ40 and about 3 times higher than that of FA40, see in the figure. For QZ40, the autogenous deformation showed an expansion after 3 days, which peaked at about 10 days and was followed only by moderate shrinkage afterwards. The possible expansion mechanisms could be reabsorption of bleeding water (hygral swelling) [58] or crystallization pressure of portlandite and ettringite [59]). The latter was not considered in the poro-elastic approach used here, where decrease of internal RH is the driving force. Besides, it is unlikely that the crystallization pressure plays a role in the expansion of the quartz system, as the pore solution is more diluted in this system compared to the pure cement system, and hence lower crystallization pressure should be expected according to [59]. On the other hand, reabsorption of bleeding water should result in increase of internal RH and hence should in principle allow to capture the hygral swelling effect with the present approach. However, no RH increase was observed in the measurements. In fact, the measured internal RH decreased constantly, albeit only moderately. This difference might be due to different geometries of the tested samples: the bulkier samples used for autogenous shrinkage measurements, filled in vertical position, may have experienced more bleeding (and hence swelling) than the miniature samples used for RH measurements.

For all prediction methods, the predicted elastic component of the autogenous shrinkage in PC and FA40 at 28 days was only about one quarter of the measured autogenous shrinkage.

The difference of the predictions according to the different poro-elastic approaches is small. The maximum difference (around 60 μm/m) occurred in PC. The difference of predictions between the Biot-Bishop

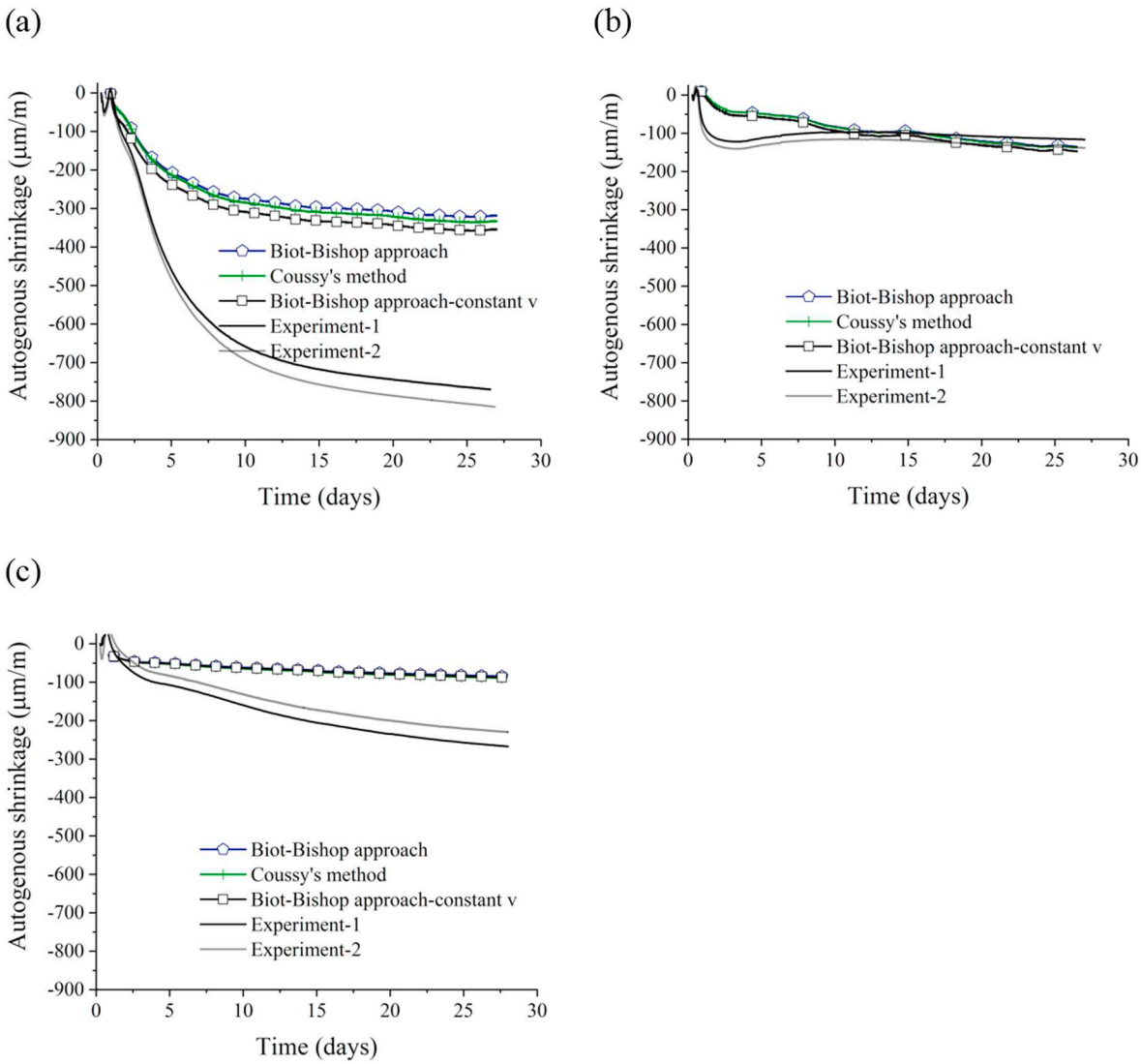

Fig. 5. Predicted elastic component of autogenous shrinkage with three different models. (a) PC; (b) QZ40; (c) FA40. Biot-Bishop model is used with either age-dependent Poisson's ratio, or with constant Poisson's ratio of 0.22.

approach and Coussy's approach is negligible, because the term due to interface energy is comparatively small at high saturation degrees [23]. It should be noted that the similar results to those predicted with the other models were found in [60] also when the model by Vlahinic et al. [61] was used. Similar predictions with different poro-elastic approaches at high RH are consistent with previous findings [60], see also [24,28]. The effect of different Poisson's ratios used in the model is higher than that caused by using different models (see Fig. 5a), however it is still relatively small compared to the overall magnitude of shrinkage.

For QZ40, the predicted result is very close to the measured autogenous shrinkage at 28 days. However, attention has to be paid to the period before 7 days, where the predicted shrinkage is much lower than the measured results. Later, swelling was measured that could not be modelled with the present approach; the good agreement of the shrinkage value at 28 days is therefore only accidental.

5.1.2. Comparison of the prediction with different saturation degree

The highest difference in the saturation degree resulting from using two extreme approaches, Powers' model (Eq. (6a)) vs. NMR combined with chemical shrinkage, excluding interlayer water (Eq. (6c)) reached 0.07. As shown in Fig. 6, such difference corresponds to a very low difference in the predicted poro-elastic strain when estimated with the Biot-Bishop approach, below 50 μm/m for the most extreme case of PC. Therefore, it can be concluded that estimating the saturation degree with the simpler approach of Powers' model does not impact the calculated poro-elastic deformation [11].

5.1.3. Comparison of the predictions with different bulk moduli

The comparison of the predicted results by using different values for the bulk modulus of the solid skeleton, K_S, is shown in Fig. 7. Again, the impact of the variation in K_S is negligible, with 50 μm/m difference between the highest bulk modulus and the lowest bulk modulus. The higher the bulk modulus of the solid skeleton, the higher the predicted elastic component of the autogenous shrinkage. Using a constant value for the bulk modulus of the solid skeleton, the prediction of the autogenous shrinkage would be slightly underestimated at later ages, because K_S would decrease due to the higher proportion of C-S-H in the solids [40].

5.2. Prediction of the visco-elastic component

In Fig. 8, the predicted visco-elastic component of the autogenous shrinkage based on generalized Kelvin-Voigt chains model is shown, in which the impact of using different visco-elastic Poisson's ratios is shown (see Section 4.3). The parameters used in the Kelvin-Voigt

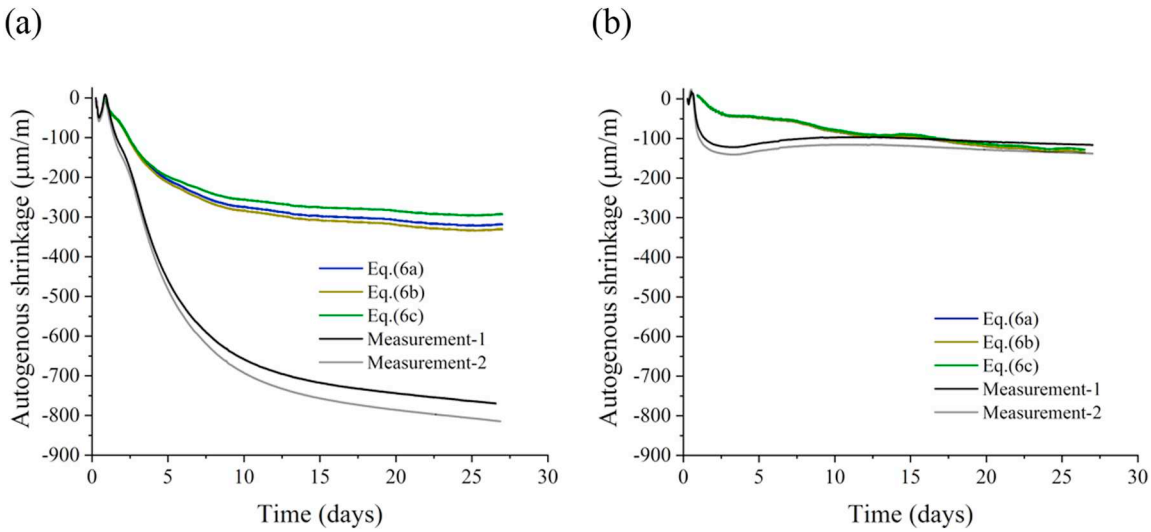

Fig. 6. Predicted elastic component of autogenous shrinkage with different saturation degrees. (a) PC; (b) QZ40 for Eq. (6a) – Powers' model, Eq. (6b) – NMR + chemical shrinkage including interlayer water, Eq. (6c) – NMR + chemical shrinkage without interlayer water.

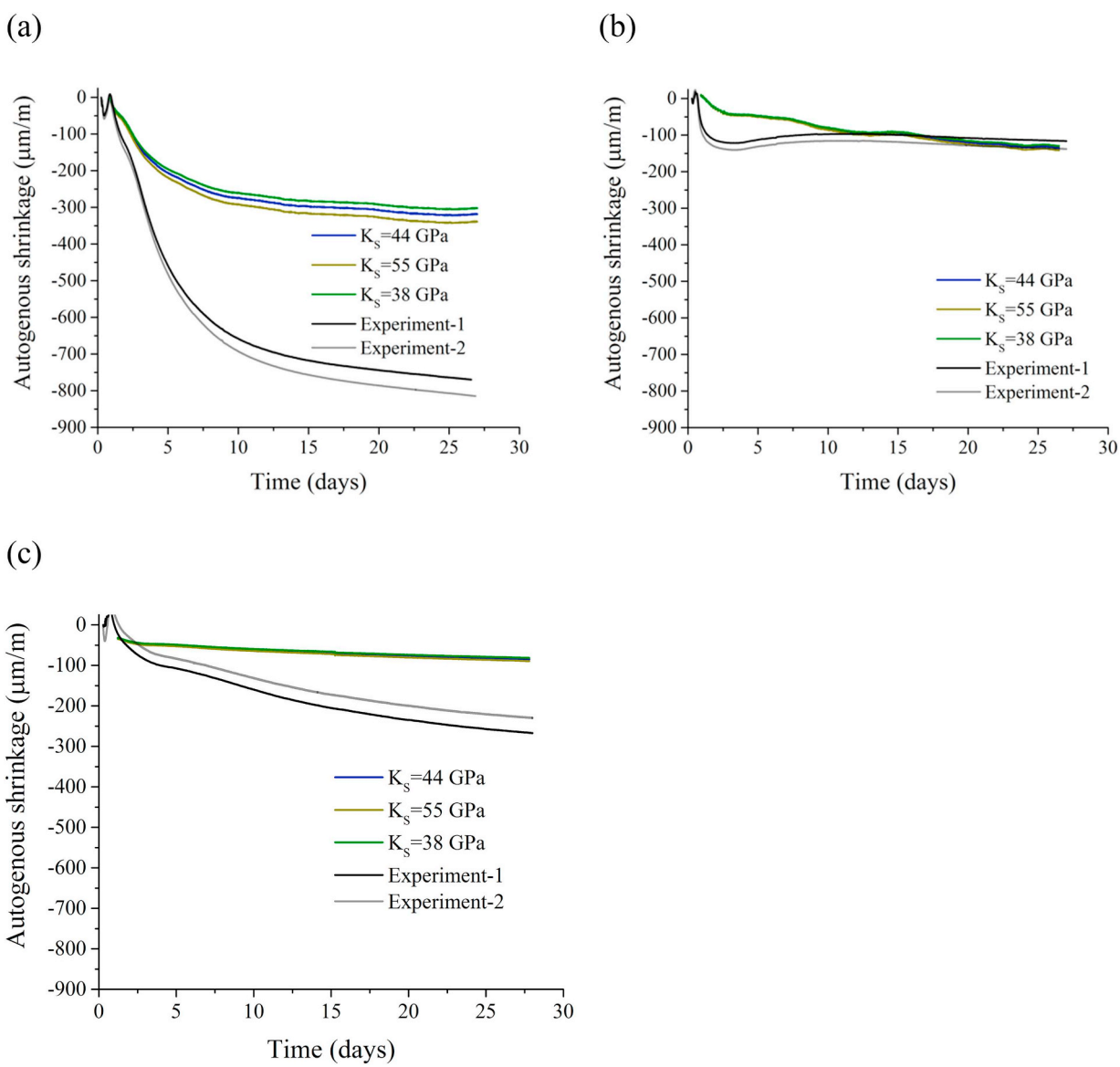

Fig. 7. Predicted elastic component (Biot-Bishop with saturation according to Eq. (6a)) of autogenous shrinkage with different values for the bulk modulus of the solid skeleton. (a) PC; (b) QZ40; (c) FA40.

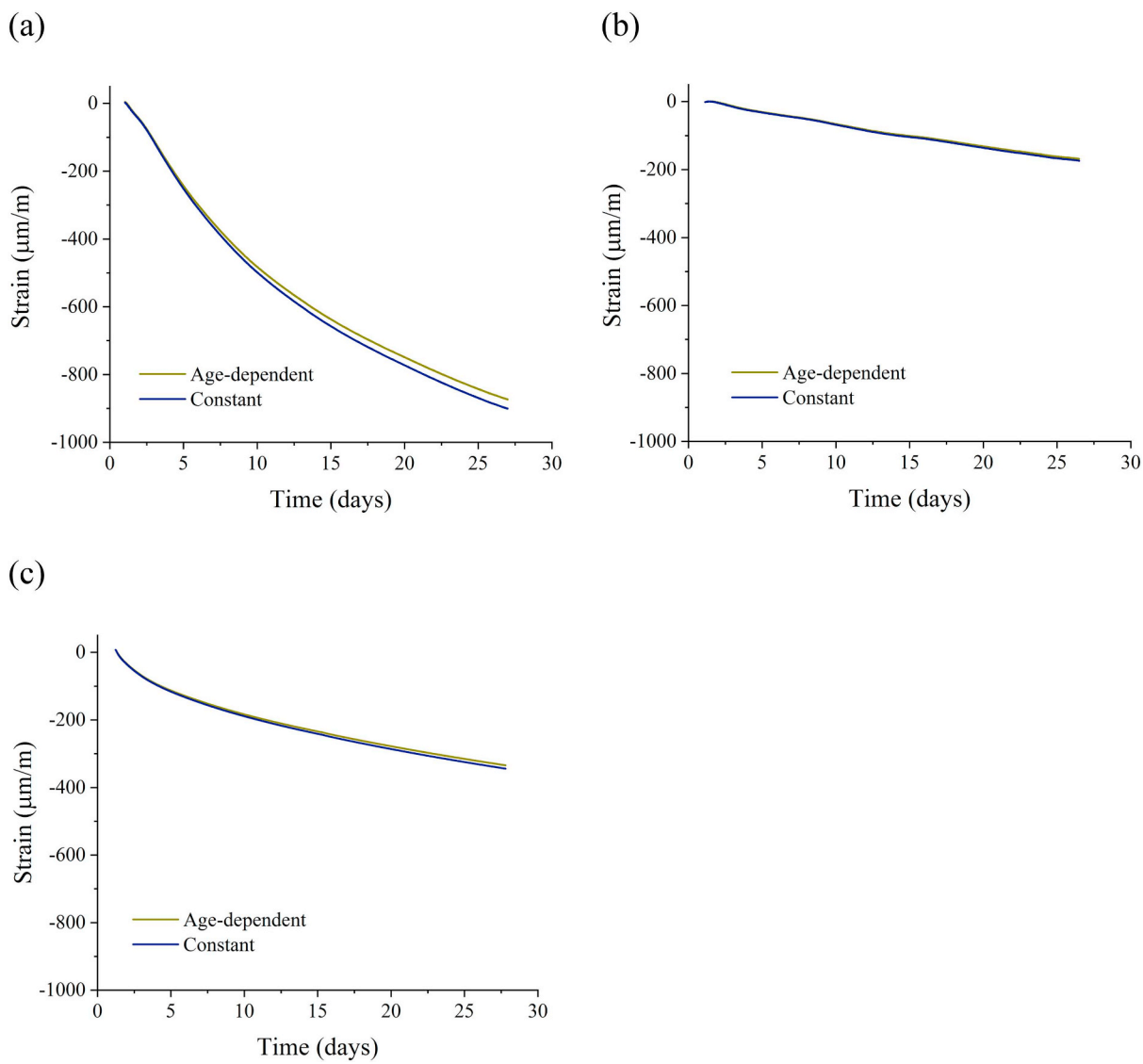

Fig. 8. Comparison of the predicted visco-elastic component of autogenous shrinkage with different visco-elastic Poisson's ratio: (a) PC; (b) QZ40; (c) FA40.

Table 2
Parameters used in the generalized Kelvin-Voigt model [44].

Sample	Unit number	Unit 1	Unit 2	Unit 3
	τ_n (days)	0.01	0.1	3.0
PC	$E_n(t)$ (MPa)	99	93	85
	η_∞ (MPa)		20	
FA40	$E_n(t)$ (MPa)	68	94	112
	η_∞ (MPa)		37	
QZ40	$E_n(t)$ (MPa)	60	140	34
	η_∞ (MPa)		35	

models are listed in Table 2. In PC and FA40, the predicted visco-elastic component is almost 2 times higher than the respective elastic components. On the other hand, in QZ40, the predicted visco-elastic component has the same magnitude as the elastic part.

As can be seen in Fig. 8, the effect of using either constant or age-dependent elastic Poisson's ratio for the visco-elastic Poisson's ratio is negligible.

5.3. Prediction of overall autogenous shrinkage

The prediction of the total autogenous shrinkage with Eq. (1), i.e. combining the poro-elastic response and the poro-visco-elastic component, is presented in Fig. 9. For all mixes, the predicted total shrinkage considerably overestimated the experimental data at later ages. In PC, a very good agreement was obtained until about 7 d. The reason of the overestimation is the poro-visco-elastic part of the deformation (see increasing creep response in Fig. 8), since the elastic part driven by pore pressure changes stabilized in all systems by about 7 d, see Fig. 5.

There are some possible explanations for the overestimation of the poro-viscoelastic part of the autogenous shrinkage:

1) as stated in [62], the uniaxial visco-elastic response of the material is most likely different from the visco-elastic response under hydrostatic load. Higher creep in uniaxial conditions may ultimately lead to higher predicted shrinkage. Also in [21] it was suggested that assuming uniaxial visco-elastic compliance for predicting the bulk compliance might lead to an overestimation.
2) Grasley and Leung [21] argued based on the different time functions of visco-elastic bulk modulus and Young modulus that assuming a constant visco-elastic Poisson's ratio is not valid. They proposed that the visco-elastic Poisson ratio should increase in time. As long as the increasing functions were derived in [57], we did not use them as they were dependent on the arbitrarily assumed functions for the visco-elastic elastic or shear moduli (as already discussed) and hence

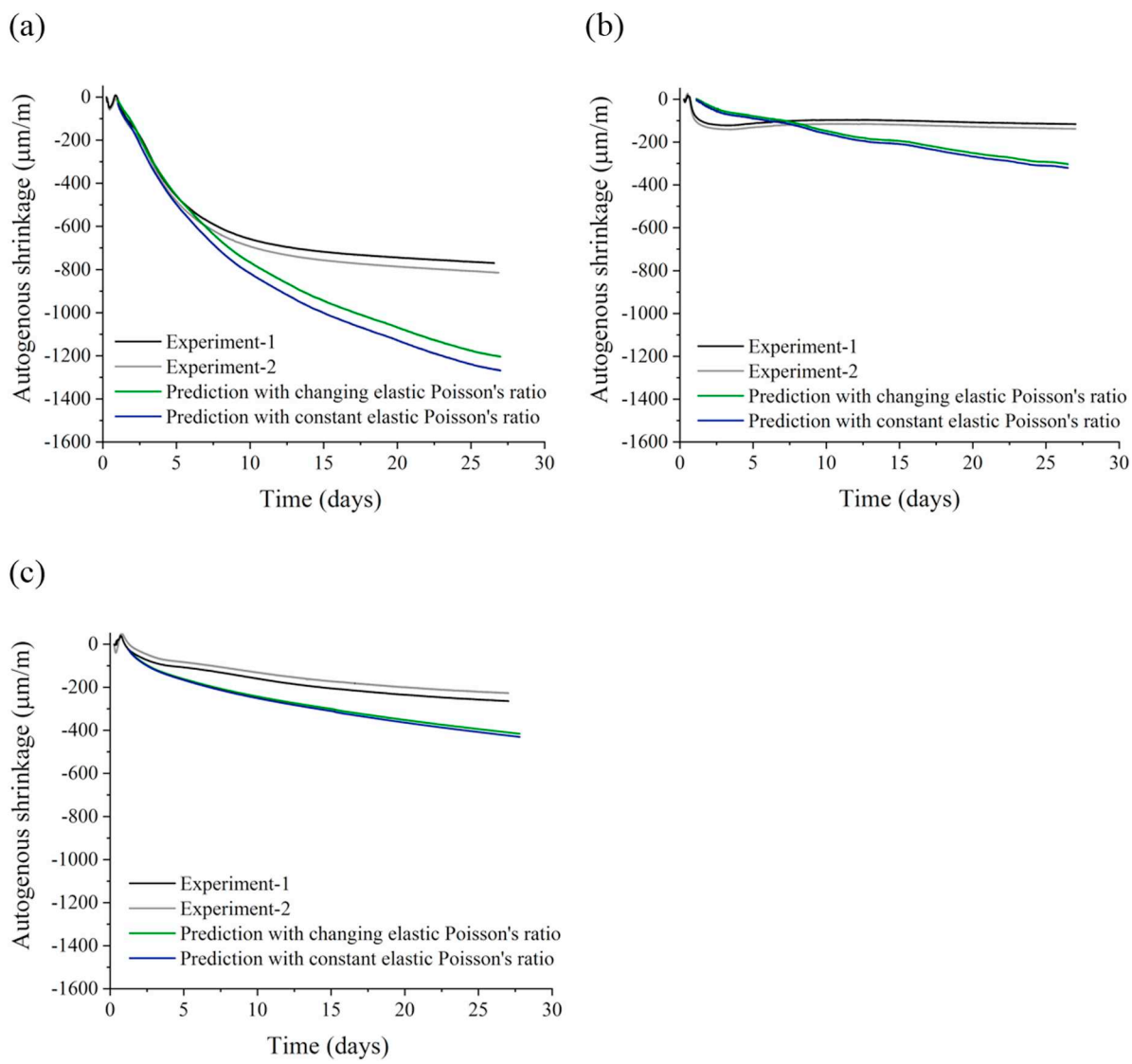

Fig. 9. Predicted autogenous shrinkage of three systems: (a) PC; (b) QZ40; (c) FA40.

could not provide any quantitative estimation here. It is however worth noting that, with an increasing Poisson's ratio, smaller creep would be predicted with Eq. (8) and hence the predictions would be closer to the experiments. Further studies, including accurate experimental determination of the Poisson's creep coefficient are necessary.

6. Conclusions

In this paper, predictions of autogenous shrinkage until 28 days based on poromechanics and including both the poro-elastic and the poro-visco-elastic response of the materials were presented. The modelling approach was based on a genuine experimental dataset on shrinkage and creep. Different poro-elastic approaches (Biot-Bishop approach and Coussy's model) were used for the elastic component. The poro-elastic simulation did not require any parameters fitting. A generalized Kelvin-Voigt chains model accounting for aging based on the measured uniaxial basic creep was used for the prediction of the poro-visco-elastic deformation. The conclusions of this study are as follows:

1. While the poro-elastic calculations underestimated the measured autogenous deformations, inclusion of the poro-visco-elastic response derived from creep experiments improved substantially the predictions. It is however noticed that, especially long-term, this approach led to overestimate the total deformations.
2. The overestimation of the predicted autogenous shrinkage at 28 days is likely because uniaxial creep measurements were used for fitting the poro-viscoelastic response. This could have led to an overestimation of creep under hydrostatic load, under which smaller creep could be expected. At the same time, an uncertainty regards the assumption of the visco-elastic Poisson's ratio equal to the elastic one. In fact, if a Poisson's ratio increasing with age were assumed, the prediction would improve.
3. The visco-elastic response outweighed the elastic response in the total prediction for the three systems studied in this paper. The differences depend on the properties of the system, such as w/c and dosage of SCMs.
4. A sensitivity study about the impact on the predicted elastic component of the autogenous shrinkage when using different a) poro-elastic models, b) bulk moduli of solid skeleton, c) Poisson's ratios and d) saturation degrees was performed. The effect of all these factors are not significant, with a maximum difference around 50 μm/m (around 7% of total autogenous shrinkage) found when using different poro-elastic models.

Acknowledgements

Zhangli Hu was supported by the China Scholarship Council (file No. 201306130062). Mateusz Wyrzykowski was supported by an SNSF Ambizione grant for the project 161414 "Role of water redistribution in creep of concrete".

Declaration of competing interests

The authors declare that they have no known competing financial interests or personal relationships that could have appeared to influence the work reported in this paper.

Appendix A

According to Powers' model and some modifications for SCMs blended systems, the volume of evaporable water of PC, QZ40and FA40 up to 28 days can be determined by assuming: non-evaporable water equal to 0.23 g/g of reacted cement and 0 g/g of reacted fly ash, chemical shrinkage equal to 6.4 ml/100 g of reacted cement and 10 ml/g of reacted fly ash [1,11,63]. The volume of chemical shrinkage V_{CS}, evaporable water V_{ew} (gel water and capillary water in Powers' model) can be calculated by following equations:

$$V_{CS} = \rho_c \bullet CS_c \bullet k \bullet (1 - p_0) \bullet (1 - \alpha_c) + \rho_f \bullet CS_f \bullet (1 - k) \bullet (1 - p_0) \bullet (1 - \alpha_f) \tag{A.1}$$

$$V_{ew} = p_0 - NE_c \bullet k \bullet (1 - p_0) \bullet (1 - \alpha_c) - NE_f \bullet (1 - k) \bullet (1 - p_0) \bullet (1 - \alpha_f) \tag{A.2}$$

where: p_0 is the initial porosity of the three systems; k is the volume fraction of cement in the binders; CS_c and CS_f are chemical shrinkage per g of reacted cement and fillers, respectively; NE_c and NE_f are non-evaporable water per gram of reacted cement and fillers; $\alpha_c$and α_f are the degree of reaction of cement and fillers, respectively. The degree of reaction of fly ash was calculated based on scanning electron microscope-energy-dispersive X-ray spectra (SEM-EDS), following the method described in [46]. The degree of hydration of the cement α_c is determined from the cumulative heat release measured by isothermal calorimetry:

$$\alpha_c = \frac{Q(t)}{Q_p} \tag{A.3}$$

where $Q(t)$ is the measured cumulative heat released at time t. Q_p is the potential heat of the cement at complete hydration, which can be determined from the mineral phases composition of the cement and from the enthalpy of complete hydration of each phase ΔH [64].

$$Q_p = \Delta H_{C_3S} \bullet C_3S\% + \Delta H_{C_2S} \bullet C_2S\% + \Delta H_{C_3A} \bullet C_3A\% + \Delta H_{C_4AF} \bullet C_4AF\%. \tag{A.4}$$

where ΔH of C_3S, C_2S, C_3A and C_4AF are equal to 517 J/g, 262 J/g, 1144 J/g or 1672 J/g, 418 J/g, respectively. $C_3S\%$, $C_2S\%$, $C_3A\%$ and $C_4AF\%$ are the percentages of the four main clinker phases in the cement.

References

[1] O.M. Jensen, P.F. Hansen, Autogenous deformation and change of the relative humidity in silica fume-modified cement paste, ACI Mater. J. 93 (1996) 539–543.
[2] O.M. Jensen, P.F. Hansen, Autogenous deformation and RH-change in perspective, Cem. Concr. Res. 31 (2001) 1859–1865.
[3] C. Pichler, R. Lackner, H.a. Mang, A multiscale micromechanics model for the autogenous-shrinkage deformation of early-age cement-based materials, Eng. Fract. Mech. 74 (2007) 34–58.
[4] X.Y. Wang, H.S. Lee, S.M. Lim, Numerical simulation of autogenous shrinkage of eco-friendly blended Portland cements using a multi-component hydration model, Mater. Sci. Forum 569 (2008) 261–264.
[5] Z. Wang, G. Li, Experimental method and prediction model for autogenous shrinkage of high performance concrete, Constr. Build. Mater. 49 (2013) 400–406.
[6] M.H. Hubler, R. Wendner, Z.P. Bažant, Statistical justification of model B4 for drying and autogenous shrinkage of concrete and comparisons to other models, Mater. Struct. 3 (2015) 797–814.
[7] Y. Li, J. Bao, Y. Guo, The relationship between autogenous shrinkage and pore structure of cement paste with mineral admixtures, Constr. Build. Mater. 24 (2010) 1855–1860.
[8] Z.P. Bažant, S. Baweja, Creep and Shrinkage Prediction Model for Analysis and Design of Concrete Structures: Model B3, (1995).
[9] R. Wendner, M.H. Hubler, Z.P. Bažant, The B4 model for multi-decade creep and shrinkage prediction, in: Mech. Phys. Creep. Shrinkage, Durab. Concr., n.d.: pp. 429–436.
[10] Q. Do, Modelling Properties of Cement Paste from Microstructure: Porosity, Mechanical Properties, Creep and Shrinkage, EPFL, 2013.
[11] P. Lura, O.M. Jensen, K. van Breugel, Autogenous shrinkage in high-performance cement paste: an evaluation of basic mechanisms, Cem. Concr. Res. 33 (2003) 223–232.
[12] C. Hua, P. Acker, A. Ehrlacher, Analyses and models of the autogenous shrinkage of hardening cement paste, Cem. Concr. Res. 25 (1995) 1457–1468.
[13] H. Chen, M. Wyrzykowski, K. Scrivener, P. Lura, Prediction of self-desiccation in low water-to-cement ratio pastes based on pore structure evolution, Cem. Concr. Res. 49 (2013) 38–47.
[14] F. Beltzung, F.H. Wittmann, Role of disjoining pressure in cement based materials, Cem. Concr. Res. 35 (2005) 2364–2370.
[15] S. Rahimi-Aghdam, E. Masoero, M. Rasoolinejad, Z.P. Bažant, Century-long expansion of hydrating cement counteracting concrete shrinkage due to humidity drop from selfdesiccation or external drying, Mater. Struct. 52 (2019) 11.
[16] D. Gawin, F. Pesavento, B.A. Schrefler, Hygro-thermo-chemo-mechanical modelling of concrete at early ages and beyond. Part II: shrinkage and creep of concrete, Int. J. Numer. Methods Eng. 67 (2006) 332–363.
[17] X. Li, Z.C. Grasley, J.W. Bullard, E.J. Garboczi, Irreversible desiccation shrinkage of cement paste caused by cement grain dissolution and hydrate precipitation, Mater. Struct. 50 (2017) 104.
[18] A. Aili, M. Vandamme, J.-M. Torrenti, B. Masson, Is long-term autogenous shrinkage a creep phenomenon induced by capillary effects due to self-desiccation? Cem. Concr. Res. 108 (2018) 186–200.
[19] Z.P. Bažant, Mathematical Modeling of Creep and Shrinkage of Concrete Material Models for Structural, (1988).
[20] C. Hua, A. Ehrlacher, P. Acker, Analyses and models of the autogenous shrinkage of hardening cement paste II. Modelling at scale of hydrating grains, Cem. Concr. Res. 27 (1997) 245–258.
[21] Z.C. Grasley, C.K. Leung, Desiccation shrinkage of cementitious materials as an aging, poroviscoelastic response, Cem. Concr. Res. 41 (2011) 77–89.
[22] A.W. Bishop, G.E. Blight, Some aspects of effective stress in saturated and partly saturated soils, Géotechnique 13 (1963) 177–197.
[23] O. Coussy, The equivalent pore pressure and the swelling and shrinkage of cement-based materials, Mater. Struct. 37 (2003) 15–20.
[24] C. Di Bella, M. Wyrzykowski, P. Lura, Evaluation of the ultimate drying shrinkage of cement-based mortars with poroelastic models, Mater. Struct. 50 (2017) 52.
[25] Z. Hu, M. Wyrzykowski, K. Scrivener, P. Lura, A novel method to predict internal relative humidity in cementitious materials by 1 H NMR, Cem. Concr. Res. 104 (2018) 80–93.
[26] C. Di Bella, M. Griffa, T.J. Ulrich, P. Lura, Early-age elastic properties of cement-based materials as a function of decreasing moisture content, Cem. Concr. Res. 89 (2016) 87–96.
[27] A.C.A. Muller, Characterization of Porosity & C-S-H in Cement Pastes by 1 H NMR, EPFL, 2014.
[28] M. Wyrzykowski, C. Di Bella, P. Lura, Prediction of drying shrinkage of cement-based mortars with poroelastic approaches – A critical review, 6th Biot Conf. Poromechanics, Paris, 2017.
[29] T.C. Hansen, Physical structure of hardened cement paste, Mater. Struct. 19 (1986) 423–436.
[30] A.C.A. Muller, K.L. Scrivener, A.M. Gajewicz, P.J. McDonald, Use of bench-top NMR to measure the density, composition and desorption isotherm of C-S-H in cement paste, Microporous Mesoporous Mater. 178 (2013) 99–103.
[31] A. Valori, P.J. McDonald, K.L. Scrivener, The morphology of C-S-H: lessons from 1H nuclear magnetic resonance relaxometry, Cem. Concr. Res. 49 (2013) 65–81.
[32] M. Wyrzykowski, P.J. Mcdonald, K. Scrivener, P. Lura, Water redistribution within the microstructure of Cementitious materials due to temperature changes studied with 1 H NMR, J. Phys. Chem. C. (2017) (acs.jpcc.7b08141).
[33] M.J. Setzer, The solid-liquid gel-system of hardened cement paste, Restor. Build. Monum. 14 (2008) 259–270.
[34] H.J.H. Brouwers, The work of Powers and Brownyard revisited: part 2, Cem. Concr. Res. 35 (2005) 1922–1936.

[35] ASTM C 642-13, Standard Test Method for Density, Absorption, and Voids in Hardened Concrete, (2013).
[36] E.P. Barett, L.G. Joyner, P.P. Halenda, The determination of pore volume and area distributions in porous substances. i. Computations from nitrogen isotherms, J. Am. Chem. Soc. 73 (1951) 373–380.
[37] A.C.A. Muller, K.L. Scrivener, A.M. Gajewicz, P.J. Mcdonald, Densification of C−S−H measured by 1 H NMR Relaxometry, J. Phys. Chem. 117 (2013) 403–412.
[38] A.P. Roberts, E.J. Garboczi, Computation of the linear elastic properties of random porous materials with a wide variety of microstructure, R. Soc. 458 (2002) 1033–1054.
[39] M. Wyrzykowski, P. Lura, Moisture dependence of thermal expansion in cement-based materials at early ages, Cem. Concr. Res. 53 (2013) 25–35.
[40] Z.C. Grasley, G.W. Scherer, D.A. Lange, J.J. Valenza, Dynamic pressurization method for measuring permeability and modulus: II. Cementitious materials, Mater. Struct. 40 (2007) 711–721.
[41] ASTM C215, Standard test method for fundamental transverse, longitudinal, and torsional resonant frequencies of concrete specimens 1, Am. Soc. Test. Mater. (2014) 1–7.
[42] Z.P. Bazant, Solidification theory for concrete creep. I: formulation, Engineering 115 (1989) 1691–1703.
[43] M. Briffaut, F. Benboudjema, J.M. Torrenti, G. Nahas, Concrete early age basic creep: experiments and test of rheological modelling approaches, Constr. Build. Mater. 36 (2012) 373–380.
[44] Z. Hu, M. Wyrzykowski, A. Hilaire, P. Lura, K.L. Scrivener, Visco-Elastic Behavior of Blended Cementitious Materials at Early Ages, submitted (2019).
[45] M. Wyrzykowski, Z. Hu, S. Ghourchian, K. Scrivener, P. Lura, Corrugated tube protocol for autogenous shrinkage measurements: review and statistical assessment, Mater. Struct. 50 (2017) 50–57.
[46] Z. Hu, A. Hilaire, J. Ston, M. Wyrzykowski, P. Lura, K. Scrivener, Intrinsic viscoelasticity of C-S-H assessed from basic creep of cement pastes, Cem. Concr. Res. 121 (2019) 11–20.
[47] ASTM C1698-09, Standard Test Method for Autogenous Strain of Cement Paste and Mortar, (2009).
[48] SN 505 262/1 Construction en béton – Spécifications complémentaires, (2003), pp. 1–28.
[49] T.C. Powers, T.L. Brownyard, Studies of the physical properties of hardened Portland cement paste, J. Am. Concr. Inst. 43 (1946) 101–132.
[50] H.J.H. Brouwers, The work of Powers and Brownyard revisited: part 1, Cem. Concr. Res. 34 (2004) 1697–1716.
[51] H.J.H. Brouwers, The work of power and Brownyard revisited: part 2, Cem. Concr. Res. 35 (2005) 1922–1936.
[52] L.F. Boswell, Z. Chen, A general failure criterion for plain concrete, Int. J. Solids Struct. 23 (1987) 621–630.
[53] O. Bernard, F.J. Ulm, E. Lemarchand, A multiscale mictomechanics-hydration model for the early-age elastic properties of cement-based materials, Cem. Concr. Res. 33 (2003) 1293–1309.
[54] M. Vandamme, The Nanogranular origin of concrete creep: a Nanoindentation investigation of microstructure and fundamental properties of calcium-silicate-hydrates, Environ. Eng. (2008) 366.
[55] A. Aili, M. Vandamme, J.M. Torrenti, B. Masson, Theoretical and practical differences between creep and relaxation Poisson's ratios in linear viscoelasticity, Mech. Time-Dependent Mater. 19 (2015) 537–555.
[56] M. Polivka, D. Pirtz, R.F. Adams, Studies of creep in mass concrete, ACI Spec. Publ. 6 (1963) 257–286.
[57] X. Li, Z.C. Grasley, J.W. Bullard, E.J. Garboczi, Computing the time evolution of the apparent viscoelastic/viscoplastic Poisson's ratio of hydrating cement paste, Cem. Concr. Compos. 56 (2015) 121–133.
[58] B.J. Mohr, K.L. Hood, Influence of bleed water reabsorption on cement paste autogenous deformation, Cem. Concr. Res. 40 (2010) 220–225.
[59] G. Sant, B. Lothenbach, P. Juilland, G. Le Saout, J. Weiss, K. Scrivener, The origin of early age expansions induced in cementitious materials containing shrinkage reducing admixtures, Cem. Concr. Res. 41 (2011) 218–229.
[60] Z. Hu, Prediction of Autogenous Shrinkage in Fly Ash Blended Cement Systems, EPFL, 2017.
[61] I. Vlahinić, H.M. Jennings, J.J. Thomas, A constitutive model for drying of a partially saturated porous material, Mech. Mater. 41 (2009) 319–328.
[62] Z.C. Grasley, D.A. Lange, The viscoelastic response of cement paste to three-dimensional loading, Mech Time-Depend Mater 11 (2007) 27–46.
[63] H. Justnes, B. Ardoullie, E. Hendrix, E. Sellevold, D. Van Gemert, The chemical shrinkage of Pozzolanic reaction products, ACI SP 179–11, 1998, pp. 191–205.
[64] H.F.W. Taylor, Cement Chemistry, Thomas Telford Publishing, 1997.